npj | climate and atmospheric science

Article

Published in partnership with CECCR at King Abdulaziz University

https://doi.org/10.1038/s41612-025-01213-7

Indian summer monsoon rainfall drives Antarctic climate and sea ice variability through atmospheric teleconnections

Check for updates

Qianghua Song[1,2,3], Chunzai Wang[1,2,4] ✉, Lei Zhang[1,2,4] & Hanjie Fan[5]

In recent decades, Antarctica has undergone significant climate change, with most studies focusing on the impact of oceanic multiscale variability on Antarctica, especially on West Antarctica. However, our research reveals that Indian summer monsoon (ISM) rainfall strongly influences the austral winter (June–August) Antarctic climate and sea ice concentration (SIC) through atmospheric teleconnections. Diabatic heating from ISM rainfall shifts the Hadley cell northward, triggering a Rossby wave train from the Mascarene Islands into Antarctica. This alters sea level pressure and induces warm advection to both East and West Antarctica, leading to widespread warming. Consequently, Antarctic SIC undergoes a tripole redistribution, with increases in the Ross and Weddell Seas, and decreases in the Amundsen and Bellingshausen Seas. These findings emphasize the importance of ISM rainfall in shaping Antarctic climate and SIC, suggesting ISM rainfall as a possible contributing factor to the record-low Antarctic SIC observed during the austral winter of 2023.

In recent decades, pronounced climatic shifts have occurred in Antarctica, with the most rapid warming observed in the western region, where surface air temperature (SAT) has risen at roughly twice the global mean pace[1–5]. Byrd Station in Central West Antarctica, for instance, has recorded a SAT increase exceeding 2.44 °C over the past 50 years[6]. These changes in temperature have significantly impacted the Antarctic sea ice concentration (SIC)[7,8]. In contrast to the continuous decline in Arctic SIC[9,10], the Antarctic SIC initially experienced a slight increase, but this tendency was masked by pronounced regional disparities in SIC trends[11]. The Amundsen Sea and Bellingshausen Sea experienced a reduction in SIC[12–14], whereas SIC increases were recorded in the Ross Sea and Weddell Sea[15,16]. The SIC increase reached its highest annual average in 2014, followed by a sharp decline in 2016, and reached a historic low in 2023[16–20]. These changes in SAT and SIC in Antarctica have significant implications for sea level rise[21,22], polar ecosystems[23,24], atmospheric circulation[25,26], and ocean circulation[27,28].

In the case of drastic climatic changes in Antarctica, natural variabilities play dominant roles, while the impact of anthropogenic forcing is comparatively minor[3,15]. The natural variabilities affecting Antarctica primarily include local circulation patterns including the circumpolar zonal wave-3 and the Southern Annular Mode[29–33], as well as remote teleconnections from beyond the Antarctic region[11]. The well-documented effect of El Niño-Southern Oscillation (ENSO) on Antarctica has given rise to the concept of connections between the tropics and the poles[11,34–38]. Tropical climate variabilities, including the tropical Atlantic sea surface temperature (SST) variability[5,39–43], the Indian Ocean Dipole (IOD)[44–46], and convection over the Maritime Continent[44,47], have been found to affect Antarctic climate and SIC by generating atmospheric Rossby waves that interact with the Amundsen Sea Low[48–50] on interannual timescales. Additionally, the SST anomalies in the extratropical southern Indian Ocean can also alter the distribution of Antarctic sea ice[51,52]. Moreover, the Pacific Quasi-Decadal Oscillation[53], the Atlantic Multidecadal Oscillation[5,41,42,54], and the Interdecadal Pacific Oscillation[38,55,56] exert significant impact on decadal variability in Antarctica. Moreover, research indicates that the pronounced warming of the tropical Atlantic alongside the moderate cooling of the equatorial Pacific over the 20th century has contributed to the centennial-scale changes in Antarctic snowfall[57]. These remote influences typically modify the Antarctic atmospheric circulation via the excitation of Rossby waves, thereby affecting Antarctic SAT and SIC[11]. In addition, recent studies have demonstrated that tropical–polar teleconnections can significantly influence the variability of atmospheric rivers over Antarctica. The atmospheric rivers carry heat and moisture from the subtropical and mid-latitude areas of the Southern Hemisphere toward Antarctica, notably impacting precipitation, SIC, and the stability of the ice shelves[58–61].

[1]State Key Laboratory of Tropical Oceanography, South China Sea Institute of Oceanology, Chinese Academy of Sciences, Guangzhou, China. [2]Global Ocean and Climate Research Center, South China Sea Institute of Oceanology, Chinese Academy of Sciences, Guangzhou, China. [3]University of Chinese Academy of Sciences, Beijing, China. [4]Guangdong Key Laboratory of Ocean Remote Sensing, South China Sea Institute of Oceanology, Chinese Academy of Sciences, Guangzhou, China. [5]School of Atmospheric Sciences, Sun Yat-sen University, Zhuhai, China. ✉e-mail: cwang@scsio.ac.cn

The Indian summer monsoon (ISM), which accounts for over 80% of annual rainfall in the ISM region, shows considerable interannual variability in atmospheric circulation and rainfall[62]. The ISM rainfall not only affects billions of local people but also interacts with climate systems across the globe through atmospheric teleconnections. Previous studies have revealed multiple modes of interaction between ISM rainfall and polar SIC, indicating that ISM rainfall responds to variations in SIC in both the Arctic and Antarctic[63–66]. Moreover, the melting of Antarctic SIC and the combined melting of both poles exert a greater impact on the ISM rainfall than Arctic sea ice melt alone[65,66]. Conversely, ISM rainfall can also modulate Arctic SIC variability[67,68]. Beyond the polar regions, ISM rainfall can trigger atmospheric teleconnections that have far-reaching impacts on the climate of other regions across the globe[69–71]. Recent research also indicates that the abnormally strong ISM rainfall in 2022 triggered quasi-stationary Rossby wave, resulting in persistent heatwaves in the Yangtze River basin[72,73] and marine heatwaves in the western North Pacific[74]. Therefore, many studies have highlighted the impact of the ISM rainfall on the climate of the Northern Hemisphere.

However, there has been limited research on the impact of the ISM rainfall on the climate of the Southern Hemisphere, particularly the Antarctic climate and SIC. Furthermore, research efforts have predominantly targeted SAT and SIC changes in West Antarctica and the Antarctic Peninsula, with East Antarctica remaining less explored, although some sectors of its ice sheet have undergone mass reduction over recent decades[75]. Our research aims to explore the impact of the ISM rainfall on Antarctica, particularly East Antarctica, and its underlying mechanisms. This study plays a vital role in enhancing predictions of climate change and sea ice distribution across Antarctica.

Results

Spatial-temporal characteristics of ISM rainfall and Antarctic SIC

To better characterize the interannual variability of ISM rainfall, we refer to the ISM rainfall index proposed in previous studies[67,68], which is defined as the regionally averaged rainfall. Based on the spatial pattern of the JJA climatological average and standard deviation of ISM rainfall (Fig. 1a, b), we define the standardized regional average JJA rainfall over 10°N–28°N, 70°E–100°E (red box in Fig. 1a) as the ISM rainfall index.

The empirical orthogonal function (EOF) analysis was conducted to extract the dominant modes of the JJA Ross-Amundsen-Bellingshausen-Weddell Seas (50°S–90°S, 120°E–10°W, Supplementary Fig. 1) SIC variability (see Methods). The leading mode (SIC-EOF1) predominantly represents a dipole pattern in sea ice, marked by opposite SIC anomalies between the Ross-Amundsen Seas and the Bellingshausen-Weddell Seas (Supplementary Fig. 2a). The first mode explains approximately 28% total variance. In contrast, the second mode (SIC-EOF2) reveals a tripole pattern (Fig. 1c), with SIC increasing in the Ross Sea and Weddell Sea and decreasing in the Amundsen-Bellingshausen Seas. The second mode accounts approximately 15% of the total variance. Additionally, unlike the almost negligible correlation between the first SIC mode and ISM rainfall index (Supplementary Fig. 2b), a significant correlation ($r = 0.50$, $p < 0.01$) is observed between the principal component (SIC-PC2) of the SIC-EOF2 and ISM rainfall index (Fig. 1d), suggesting that the ISM rainfall may drive the aforementioned tripole redistribution pattern. By analyzing the spatial-temporal characteristics of ISM rainfall and Antarctic SIC, we preliminarily conclude that ISM rainfall can influence the distribution of Antarctic SIC and, potentially, the Antarctic climate.

The impact of ISM rainfall on Antarctica

We next examine the effects of the ISM rainfall on the JJA Antarctic climate and explore the potential mechanisms behind these effects. To do so, we first regressed JJA Antarctic SAT and SIC onto the ISM rainfall index. Significant warming is observed in East Antarctica (70°S–90°S, 0°–90°E), extending to the central part of the Antarctic continent (Fig. 2a). In addition, warming is also detected in West Antarctica (65°S–90°S, 60°W–160°W). In contrast, the Ross Sea and Weddell Sea experience marked cooling. Concurrently,

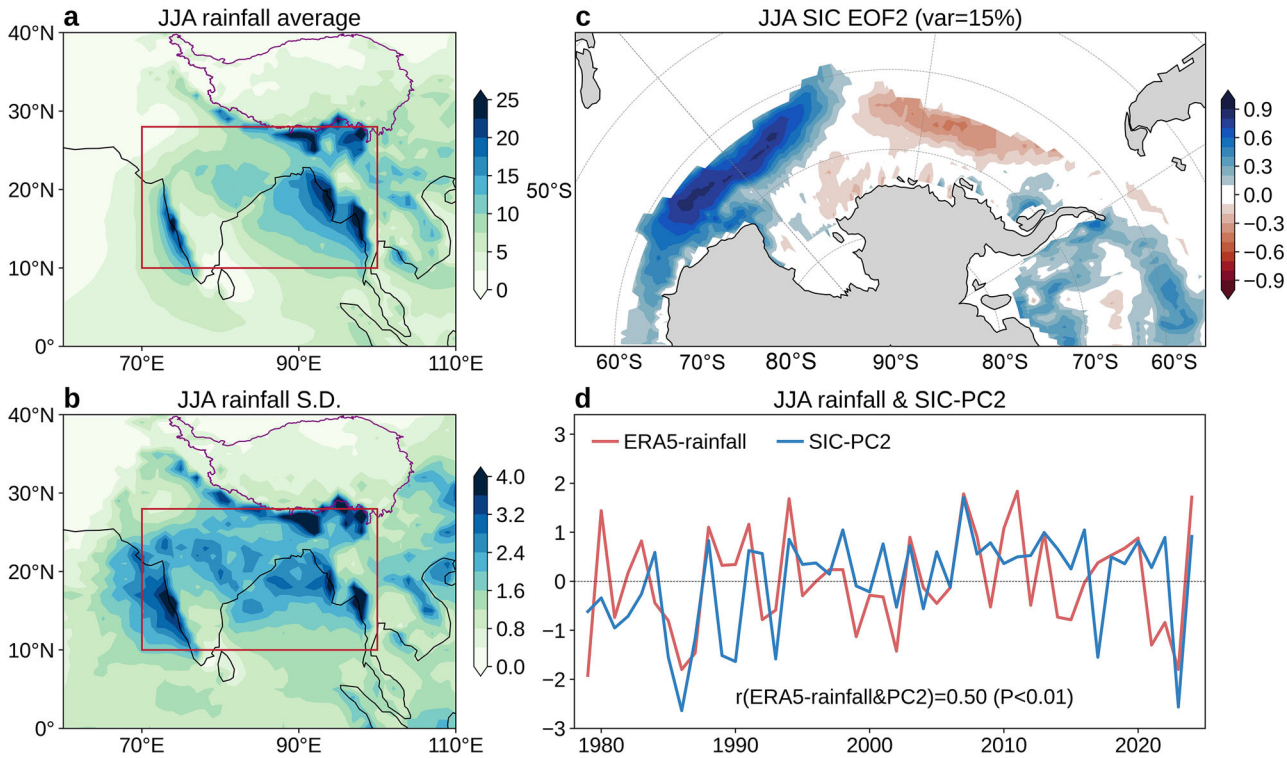

Fig. 1 | The main spatial-temporal characteristic of Indian summer monsoon (ISM) rainfall and Antarctic sea ice concentration. The **a** climatological average and **b** standard deviation of June–August ISM rainfall (unit: mm/day). The red box (10°N–28°N, 70°E–100°E) in (**a**, **b**) indicates the region with high rainfall and variability, and the standardized regional average JJA rainfall within this region is defined as the ISM rainfall index. **c** The second empirical orthogonal function (EOF) modes of JJA Antarctic sea ice concentration (SIC-EOF2). **d** The correlation coefficient between principal component (SIC-PC2, blue curve) of the SIC-EOF2 and ISM rainfall index (red curve) is 0.50 ($p < 0.01$). The purple contours in (**a**, **b**) indicate the Tibetan Plateau.

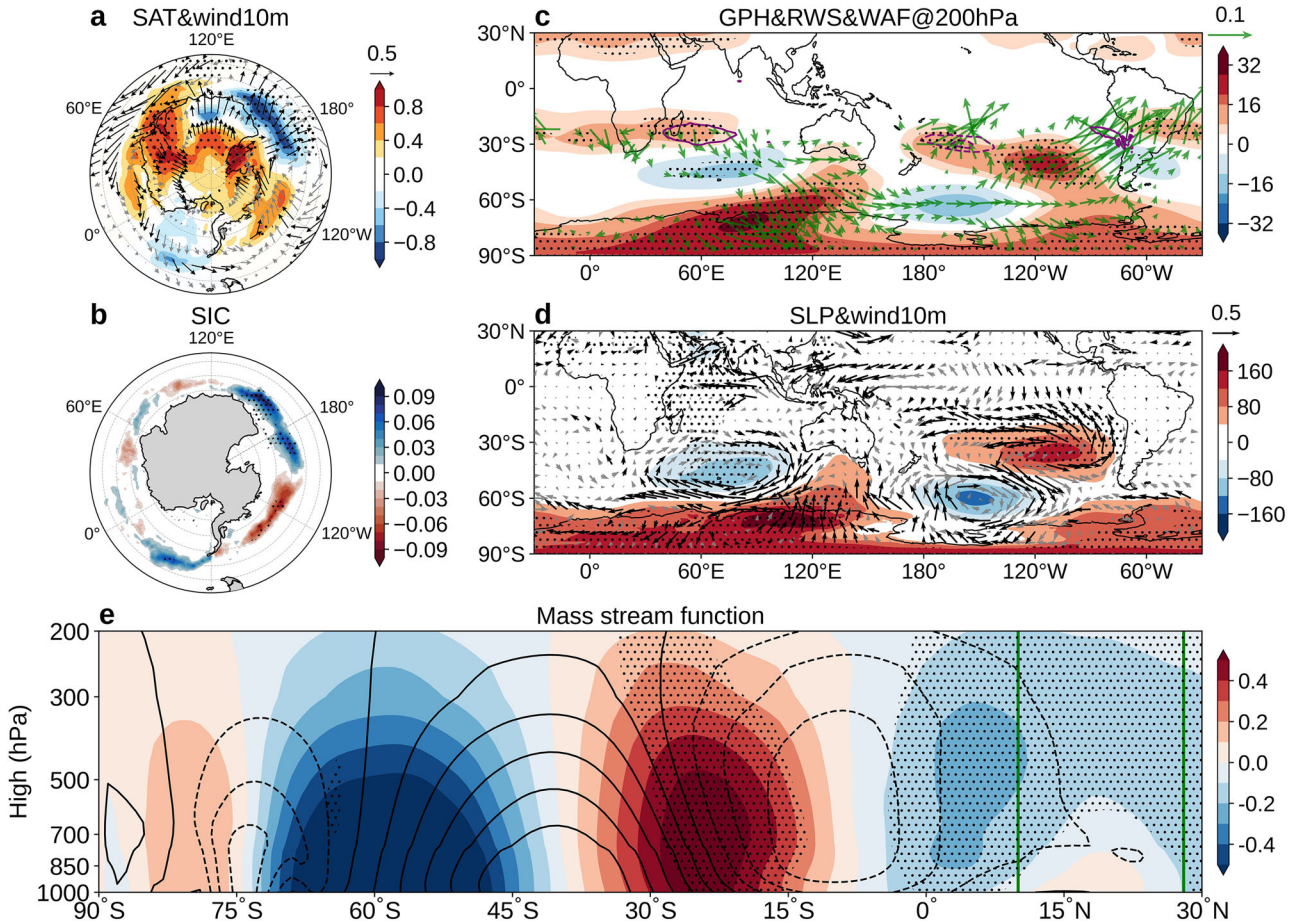

Fig. 2 | Impact of the Indian summer monsoon (ISM) rainfall on Antarctica. June–August (**a**) surface air temperature (SAT, shading, unit: °C) and 10 m wind speed (vectors, unit: m s^{-1}), **b** sea ice concentration (SIC, unit: 1), **c** 200-hPa geopotential height (shading, unit: gpm), Rossby wave source (RWS, purple contour, positive solid and negative dashed, zero line omitted, contour interval: 1, unit: 10^{-11} s^{-2}) and wave activity flux (WAF, green vectors, values smaller than 0.01 are filtered out, unit: m^2 s^{-2}), **d** sea level pressure (SLP, shading, unit: Pa) and 10 m wind speed (vectors, unit: m s^{-1}), and **e** mass stream function averaged over 60°E–100°E (shading, unit:10^9 kg s^{-1}) regressed onto ISM rainfall index. The contours in (**e**) represent the climatological mean mass stream function for JJA during 1979–2024 (positive solid and negative dashed, contour interval: 1.5, unit: 10^9 kg s^{-1}). The dotted areas in the shading, as well as the black vectors, indicate significance at the 95% confidence level. The two green lines in (**e**) denote the latitudinal extent of the ISM region (10°N–28°N). Circulation is clockwise (anticlockwise) around positive (negative) mass stream function.

significant changes in Antarctic SIC are observed, with a SIC increase in the Ross Sea and Weddell Sea and a SIC decrease in the Amundsen-Bellingshausen Seas, forming a tripole pattern (Fig. 2b). This fully explains the significant correlation between the ISM rainfall index and SIC-PC2, in view of SIC-EOF2 representing the tripole pattern of JJA SIC variation in the Ross-Amundsen-Bellingshausen-Weddell Seas.

Since ENSO and IOD has a significant impact on Antarctic climate and SIC[34–38], as well as on ISM rainfall[62,76,77], the composite analysis was conducted to eliminate the influence of ENSO and IOD and obtain the pure impact of ISM rainfall on Antarctica. We first examined extreme cases by selecting years with high (> 1) and low (<−1) ISM rainfall index (Supplementary Fig. 3). After excluding years where strong ENSO or IOD events occurred, there are four years identified for both high and low ISM rainfall index categories. We then compared the JJA SAT, SIC, and surface wind between these high and low ISM rainfall index years. The differences closely resemble the regression results, displaying that East Antarctica (60°S–90°S, 0°–100°E) warmed by more than 4 °C and West Antarctica (65°S–90°S, 60°W–160°W) warmed by nearly 3 °C (Supplementary Fig. 4a), with the SIC variation exceeding 30% (Supplementary Fig. 4b), highlighting the significant impact of the extreme ISM rainfall on Antarctica.

Mechanisms of ISM rainfall affecting the Antarctica

So how does ISM rainfall affect the Antarctic climate and SIC? Regression of the Southern Hemisphere's JJA geopotential height, sea level pressure (SLP) and surface wind onto ISM rainfall index reveals an atmospheric teleconnection between ISM rainfall and Antarctica. Specifically, in the upper atmosphere, a Rossby wave train originates near the Mascarene Islands (Rossby wave source and wave activity flux in Fig. 2c), travels across the southern Indian Ocean, passes over East Antarctica (60°S–90°S, 60°E–120°E), extends to the Ross-Amundsen Seas, and forms two branches: the northern branch eventually reaches the South Pacific, while the southern branch reaches the Antarctic Peninsula (Fig. 2c). Due to the barotropic structure of atmospheric teleconnections[78–80], a corresponding Rossby wave train also emerges in the lower atmosphere, which markedly increases the SLP over East Antarctica (60°S–90°S, 60°E–120°E) and Antarctic Peninsula while decreasing the SLP over the Ross-Amundsen Seas, thereby strengthening the Amundsen Sea Low (Fig. 2d). The tripole SLP pattern in Antarctica induces an anticyclone circulation (anticlockwise) over East Antarctica (60°S–90°S, 60°E–120°E) and Antarctic Peninsula as well as a cyclone circulation (clockwise) in the Ross-Amundsen Seas, respectively (vectors in Fig. 2a).

The surface northerly wind on the west side of the anticyclone over East Antarctica (60°S–90°S, 60°E–120°E) transports warm air from low latitudes toward the Antarctic continental center, resulting in significant warm advection (Fig. 2a). Conversely, the surface southerly wind on the east side of the anticyclone combined with surface southerly wind on the west side of the cyclone in the Ross-Amundsen Seas form offshore winds, leading to significant cold advection in the Ross Sea. The surface northerly wind on the

east side of the cyclone, combined with the surface northerly wind on the west side of the Antarctic Peninsula anticyclone, induces warm advection, resulting in warming of the Amundsen-Bellingshausen Seas. In contrast, the offshore wind on the east side of the Antarctic Peninsula anticyclone leads to cooling in the Weddell Sea. The presence of offshore and onshore winds not only induces temperature advection, altering the SAT over the Antarctic continent, but also significantly affects SIC, which is the SIC tripole redistribution mentioned above (Fig. 2b). The Rossby wave train in the Southern Hemisphere is more pronounced in the differences in JJA geopotential height and SLP between high and low ISM rainfall index years (Supplementary Fig. 4c, d). Correspondingly, a strong anticyclone develops over East Antarctica (60°S–90°S, 60°E–120°E) and Antarctic Peninsula, and a strong cyclone develops over the Ross-Amundsen Seas. This indicates that the wave train in the Southern Hemisphere induced by ISM rainfall can occur independently of ENSO and IOD influences.

However, the impact of ISM rainfall in the Northern Hemisphere on Antarctica cannot be attributed solely to atmospheric Rossby wave train. The mechanisms also involve the atmospheric meridional overturning circulation adjustment, which can cross the equator. During normal ISM rainfall index years, the ascending branch of the JJA Hadley cell (contours in Fig. 2e) in the Indian Ocean is located slightly north of the equator, while the descending branch is situated over the Mascarene Islands in the southern Indian Ocean, forming the Mascarene High. The regression of the JJA mass stream function, averaged over the region 60°E–100°E, representing the atmospheric meridional overturning circulation, onto the ISM rainfall index reveals that the Hadley cell's ascending branch shifts further north under the influence of ISM rainfall, moving closer to the ISM region compared to the normal meridional overturning circulation (Fig. 2e). The descending branch of the Hadley cell in the southern Indian Ocean also shifts northward, causing the Mascarene High to migrate north and generating a meridional pressure gradient. Additionally, the northward shift of the Hadley cell's descending branch leads to subtropical convergence, and the interaction with intense zonal wind shear (Supplementary Fig. 5) results in anomalous Rossby wave sources along the edge of the subtropical jet[11,81].

As a result, a Rossby wave train originating from the Mascarene Islands propagates southwestward toward Antarctica, extending through the Ross-Amundsen Seas and into the Antarctic Peninsula and South Pacific. The northward shift of the Hadley cell under the influence of ISM rainfall is more apparent in the differences in the JJA mass stream function between high and low ISM rainfall index years (Supplementary Fig. 4e).

Numerical model experiments

To provide further evidence for our proposed mechanism whereby ISM rainfall can affect Antarctic climate via atmospheric teleconnection, we conducted atmospheric general circulation model (Community Atmospheric Model version 5, CAM5) experiments forced with the observed JJA climatological average diabatic heating in the ISM rainfall index region (10°N–28°N, 70°E–100°E, see Methods). The CAM5 results show that the ISM rainfall diabatic heating substantially modifies atmospheric circulation, generating a Rossby wave train that extends from the Mascarene Islands to Antarctica and reaches the Antarctic Peninsula and South Pacific closely resembling the observed results (Fig. 3a). The SLP also undergoes significant changes as the Rossby wave propagates, influencing surface wind over Antarctica (Fig. 3b). The onshore wind induces warm advection to both East (60°S–90°S, 60°E–150°E) and West (70°S–90°S, 60°W–160°W) Antarctica, thereby heating the Antarctic continent (Fig. 3c). Conversely, the offshore wind in the Ross Sea and Weddell Sea brings cold air from the Antarctic center, creating cold advection and leading to cooling. Thus, the CAM5 results confirm our hypothesis that ISM rainfall can indeed impact the JJA Antarctic climate.

Furthermore, the model results confirm the triggering mechanism of the Rossby wave located in the Southern Hemisphere. Consistent with the observational results, the ascending motion in the ISM region is significantly enhanced by the diabatic heating associated with ISM rainfall, leading to a further northward shift of the Hadley cell ascending branch and a northward movement of its descending branch in the southern Indian Ocean (Fig. 3d). The northward shift of the descending branch interacts with the strong wind shear of the subtropical jet, thereby triggering a Rossby wave train that propagates toward Antarctica and impacts the Antarctic climate.

Discussion

In this study, we demonstrate that the JJA ISM rainfall, located in the Northern Hemisphere, significantly influences the JJA Antarctic climate and SIC through atmospheric teleconnection mechanisms (Fig. 4). The diabatic heating released by the Indian summer monsoon rainfall causes the Hadley cell to shift northward, which in turn triggers a Rossby wave train propagating from the Mascarene Islands across the southern Indian Ocean to Antarctica. The Rossby wave changes the SLP, leading to warm advection to both East and West Antarctica along with cold advection to the Ross Sea and Weddell Sea. Owing to the effects of temperature advection, warming occurred across nearly the entire Antarctic continent. Simultaneously, the SIC in the Ross-Amundsen-Bellingshausen-Weddell Seas region exhibited a tripole distribution pattern driven by the surface wind stress and temperature advection, marked by a SIC increase in the Ross Sea and Weddell Sea and a SIC decrease in the Amundsen-Bellingshausen Seas. The mechanisms have also been consistently reproduced in CAM5 model experiments.

During the 2023 austral winter, Antarctic SIC experienced an unprecedented reduction, with a loss of 2.33 million square kilometers in sea ice extent in June, twice the size of the previous June record[18]. The decline in Antarctic SIC increased ocean heat loss and heightened the frequency of atmospheric storms, severely impacting air-sea interaction in the Southern Ocean and the broader climate system[20]. However, we observed that the certain anomalies in Antarctic SAT and SIC during the JJA 2023 exhibited a opposite pattern compared to the changes caused by the ISM rainfall (Supplementary Fig. 6a, b). Specifically, the Ross-Amundsen-Bellingshausen-Weddell Seas SIC anomalies during the JJA 2023 closely matched the SIC-EOF2 mode (Fig. 1c), exhibiting a distinct tripole pattern. Simultaneously, the atmospheric circulation in the Southern Hemisphere also exhibits anomaly patterns partially opposite to those associated with ISM rainfall (Supplementary Fig. 6c, d), with some Rossby waves originating from the Mascarene Islands in the southern Indian Ocean (Rossby wave source and wave activity flux in Supplementary Fig. 6c). Interestingly, both the ISM rainfall index and SIC-PC2 reached their lowest values in 2023 (Fig. 1d). During the JJA 2023, strong ENSO and IOD events were also developing—both known to exert substantial influences on Antarctic SIC[11,34,35,45,46]. Therefore, we speculate that the record-low Antarctic SIC during the austral winter of 2023 may have been associated with ENSO, IOD, and ISM rainfall on interannual timescales. However, the relative quantitative contributions of these three factors to the SIC reduction merit further investigation.

In fact, some previous studies have already acknowledged the connection between Antarctic SIC and the ISM rainfall[64,82,83]. However, all of their viewpoints suggest that Antarctic SIC influences the ISM rainfall[82,83], or that Antarctic SIC indirectly affects the ISM rainfall through its interaction with the ENSO[64]. This study provides a complementary perspective to previous conclusions by demonstrating that the ISM rainfall can influence variability in Antarctic SIC through atmospheric teleconnections, and that such teleconnections can exist independently of ENSO and IOD. Therefore, our findings are of great significance for reinterpreting the two-way teleconnection between Antarctic SIC and ISM rainfall.

Regarding the factors influencing Antarctic SAT and SIC, most studies have focused on the teleconnection patterns generated by interannual and interdecadal ocean variability[3,5,11,37,44,53]. Our research, however, reveals the significant impact of the Northern Hemisphere monsoon system on Antarctica, indicating that ISM rainfall plays a critical role in shaping Antarctic climate and SIC. Additionally, rainfall in other monsoon systems also generates substantial diabatic heating, which affects global atmospheric

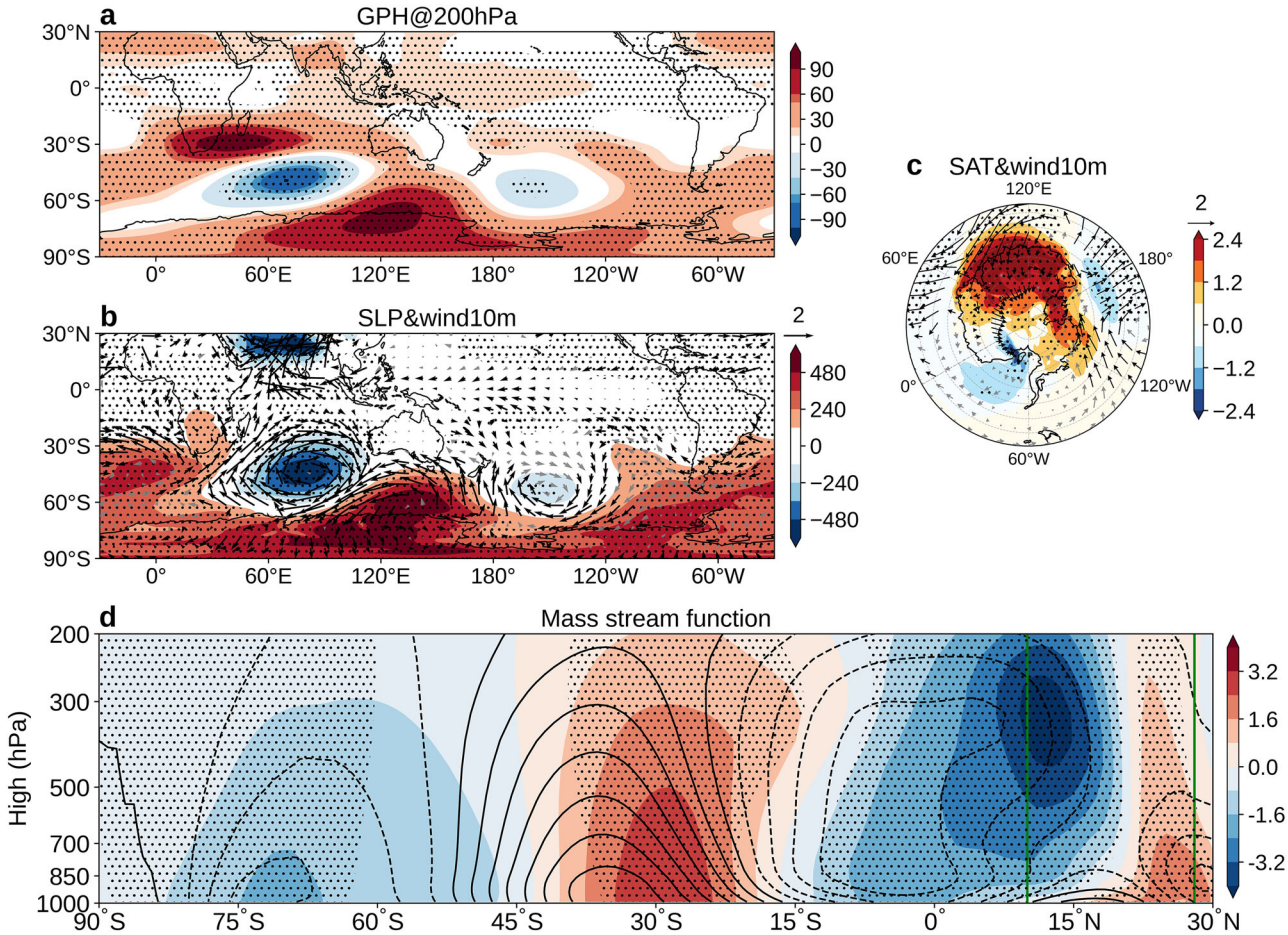

Fig. 3 | Atmospheric model experiments. Differences in June–August **a** 200-hPa geopotential height (unit: gpm), **b** sea level pressure (SLP, shading, unit: Pa) and 10 m wind speed (vectors, unit: m s^{-1}), **c** surface air temperature (SAT, shading, unit: °C) and 10 m wind speed (vectors, unit: m s^{-1}), and **d** mass stream function averaged over 60°E–100°E (shading, unit: 10^9 kg s^{-1}) between the HEATING experiment and the CTL experiment. The contours in (**d**) represent the climatological mean mass stream function for JJA in CTL experiment (positive solid and negative dashed, contour interval: 1, unit: 10^9 kg s^{-1}). The dotted areas in the shading, as well as the black vectors, indicate significance at the 95% confidence level. The two green lines in (**d**) denote the latitudinal extent of the Indian summer monsoon region (10°N–28°N). Circulation is clockwise (anticlockwise) around positive (negative) mass stream function.

circulation[69]. As such, the potential influence of Northern Hemisphere monsoon rainfall on the climate of the Southern Hemisphere, especially Antarctica, warrants further investigation. Moreover, some studies have indicated that relatively moist air transported by atmospheric rivers from low latitudes can enhance downward longwave radiation through increased cloud cover, leading to additional surface warming[58–61]. Consequently, aside from the effects of temperature advection, ISM rainfall can also influence atmospheric river activity, which subsequently modifies cloud-induced longwave radiation and ultimately affects surface air temperature and sea ice distribution over Antarctica.

Most studies have primarily focused on West Antarctica and the Antarctic Peninsula[1,2,5,6,11], with fewer investigations conducted on East Antarctica. Our findings not only enhance the understanding of climate change in West Antarctica but also highlight the impact of the ISM rainfall on East Antarctica SAT. Moreover, ISM rainfall significantly contributes to a tripole distribution pattern of Antarctic SIC—characterized by a SIC increase in the Ross Sea and Weddell Sea and a SIC decrease in the Amundsen-Bellingshausen Seas—consistent with the observed SIC trend from 1979 to 2015[11]. As future ISM rainfall and the frequency of extreme rainfall events are also expected to increase[84–87], the tripole distribution of Antarctic SIC will become more pronounced. Furthermore, East Antarctica may face an increased risk of warming, while the already severely warm West Antarctica could experience even more dramatic temperature rises.

Methods

Data sets and indices

In this study, we employ the fifth-generation atmospheric reanalysis dataset (ERA5) from the European Center for Medium-Range Weather Forecasts[88]. The monthly ERA5 reanalysis data, at a spatial resolution of 1° × 1° and covering 1979–2024, include precipitation, geopotential, horizontal wind, sea level pressure, and air temperature. The Hadley Centre Sea Ice and Sea Surface Temperature dataset[89], obtained from the Met Office Hadley Centre, provides monthly SST and sea ice data at 1° × 1° resolution for the period 1979–2024.

We use the Niño 3.4 SST index—defined as the standardized average SST anomaly over the region 5°S–5°N and 170°W–120°W—to represent ENSO variability. The IOD is quantified using the Dipole Mode Index (DMI), calculated as the standardized difference in SST anomalies between the western equatorial Indian Ocean (10°S–10°N, 50°E–70°E) and the eastern equatorial Indian Ocean (10°S–0°, 90°E–110°E).

To characterize the interannual variability of ISM rainfall, we defined the standardized regional average JJA rainfall over 10°N–28°N, 70°E–100°E as the ISM rainfall index, based on the spatial pattern of the climatological average and standard deviation of JJA rainfall in the ISM region (Fig. 1a, b). Notably, although the spatial extent of our ISM rainfall index is slightly smaller than that used in previous studies (10°N–30°N, 70°E–105°E)[67,68], the two ISM rainfall indices show almost no difference ($r = 0.98$, $p < 0.01$). Furthermore, we defined years with the ISM rainfall index greater than 1 as

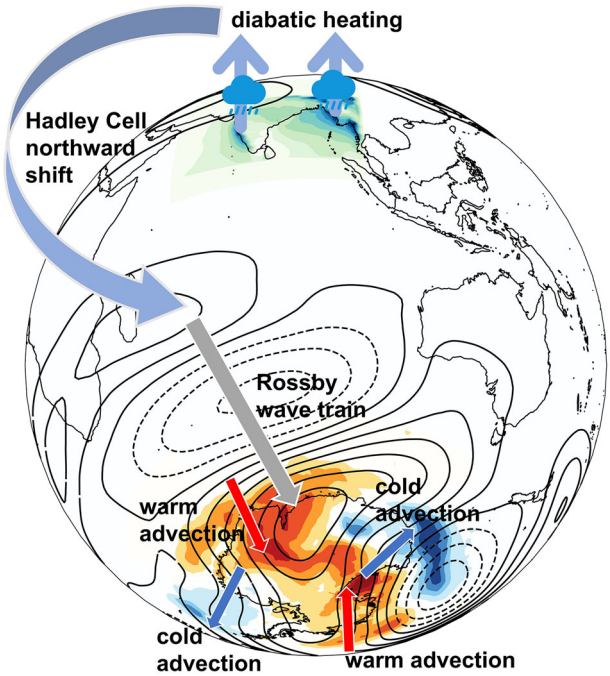

Fig. 4 | Schematic representation of the Indian summer monsoon rainfall's impact on Antarctica. The diabatic heating of June–August Indian summer monsoon rainfall causes the northward movement of the Hadley cell, triggering a Rossby wave train (contour) that propagates from the Mascarene Islands into Antarctica. The Rossby wave train alters sea level pressure and introduces warm advection (red vector in Antarctica) to both East and West Antarctica, while concurrently causing cold advection (blue vector in Antarctica) to the Ross Sea and Weddell Sea. The surface wind and temperature advection significantly influence the June–August Antarctic surface air temperature (shading in Antarctica) and sea ice.

high ISM rainfall index years, and those with the index less than −1 as low ISM rainfall index years. From these high and low ISM rainfall index years, we further excluded years with concurrent ENSO or IOD events. Ultimately, 8 extreme ISM rainfall index years were selected for composite analysis: 1991, 2007, 2011, and 2024 as high ISM rainfall index years, and 1979, 1986, 2002, and 2021 as low ISM rainfall index years.

EOF analysis of Antarctic SIC

To more objectively describe the spatial-temporal patterns of JJA Antarctic SIC, we conducted EOF analysis to capture the dominant modes of JJA Antarctic SIC in the region of high SIC variability, which is the Ross-Amundsen-Bellingshausen-Weddell Seas (50°S–90°S, 120°E–10°W). We extracted the first two EOF modes (SIC-EOF1 and SIC-EOF2) and the corresponding principal components (SIC-PC1 and SIC-PC2). The first mode explains approximately 28% of the variance, and the second mode explains 15%.

Rossby wave source

Anomalous convection associated with ISM rainfall can induce vertical motion anomalies, which in turn generate upper-level perturbations that act as a source of anomalous vorticity, denoted by the Rossby wave source (RWS). According to Sardeshmukh and Hoskins[81], the RWS calculation formula is as follows:

$$RWS = -\vec{\mathbf{V}}_\chi \cdot \nabla\zeta - \zeta D \approx -\vec{\mathbf{V}}_\chi{}' \cdot \nabla\bar{\zeta} - \bar{\zeta}D' \quad (1)$$

Here, $\vec{\mathbf{V}}_\chi$ denotes the divergent portion of the horizontal wind, ∇ is the horizontal gradient operator, ζ stands for absolute vorticity, and D indicates horizontal wind divergence. Overbars and primes signify the climatological mean and perturbation, respectively. The RWS can be effectively represented by its linearized components: S1 ($-\vec{\mathbf{V}}_\chi{}' \cdot \nabla\bar{\zeta}$), describing the advection of mean absolute vorticity by anomalous divergent flow; and S2 ($-\bar{\zeta}D'$), the vortex stretching term responsible for vorticity generation due to anomalous divergence. This study focuses on S1, as it is more effective in triggering extratropical teleconnections in response to tropical heating[46,81].

Atmospheric wave activity flux

The propagation of Southern Hemisphere atmospheric Rossby waves during JJA 2023 was analyzed using the wave activity flux formulation of Takaya and Nakamura[90]. The following is the calculation formula:

$$\vec{\mathbf{W}}_\mathbf{h} = \frac{p\cos\varphi}{2\left|\vec{\mathbf{U}}_c\right|}\begin{pmatrix} \frac{u_c}{a^2\cos^2\varphi}\left[\left(\frac{\partial\psi'}{\partial\lambda}\right)^2 - \psi'\frac{\partial^2\psi'}{\partial\lambda^2}\right] + \frac{v_c}{a^2\cos\varphi}\left[\frac{\partial\psi'}{\partial\lambda}\frac{\partial\psi'}{\partial\varphi} - \psi'\frac{\partial^2\psi'}{\partial\lambda\partial\varphi}\right] \\ \frac{u_c}{a^2\cos\varphi}\left[\frac{\partial\psi'}{\partial\lambda}\frac{\partial\psi'}{\partial\varphi} - \psi'\frac{\partial^2\psi'}{\partial\lambda\partial\varphi}\right] + \frac{v_c}{a^2}\left[\left(\frac{\partial\psi'}{\partial\varphi}\right)^2 - \psi'\frac{\partial^2\psi'}{\partial\varphi^2}\right] \end{pmatrix} \quad (2)$$

The T-N wave activity flux vector is denoted as $\vec{\mathbf{W}}_\mathbf{h}$, where φ refers to latitude, and λ refers to longitude. The climatological mean horizontal wind vector, $\vec{\mathbf{U}}_c = (u_c, v_c)$, comprises the mean zonal and meridional wind components. The perturbation stream function is expressed as ψ', where a refers to the Earth's radius and p is defined as pressure/1000 hPa. The climatological mean and perturbation values were computed for the period 1979–2024.

Atmospheric diabatic heating

During the formation process of ISM rainfall, a large amount of diabatic heating is released, which in turn influences the atmospheric circulation. However, existing observational data for the diabatic heating are not available. Therefore, it is necessary to deduce the diabatic heating rate from the air temperature. Here, we refer to deduce the diabatic heating on the basis of the calculation formula proposed by Yanai[91,92]:

$$Q_1 = C_p\frac{\partial T}{\partial t} - C_p(\omega\sigma - \vec{\mathbf{V}}\cdot\nabla T) \quad (3)$$

$$\sigma = \left(\frac{RT}{C_p p}\right) - \left(\frac{\partial T}{\partial p}\right) \quad (4)$$

Here, $C_p = 1004.7\ \mathrm{J\,kg^{-1}\,K^{-1}}$ is the specific heat capacity at constant pressure, T represents the air temperature and t stands for time. Vertical velocity is indicated by ω. Static stability is denoted by σ, the gas constant ($287\ \mathrm{J\,kg^{-1}\,K^{-1}}$) by R, pressure by p, the horizontal wind by $\vec{\mathbf{V}}$, and ∇ stands for the horizontal gradient operator.

Atmospheric general circulation model experiments

In this study, we employed the CAM5[93], the atmospheric module of the Community Earth System Model (CESM) version 1.2.2, developed by the National Center for Atmospheric Research (NCAR), to validate our proposed mechanism. The model has been extensively validated in previous studies and is considered reliable for simulating atmospheric responses induced by ISM rainfall[72,74,94].

We conducted two sets of experiments at the 0.9° latitude×1.25° longitude (f09g16) horizontal resolution, with 30 vertical levels. The first set corresponds to the control experiment (CTL), which is forced by the climatological annual cycle of SST and sea ice over the period 1979–2024. The CTL simulation is freely integrated for 30 years. We use the first 5 years as spin-up, and the subsequent 25 years are utilized to generate an ensemble mean, minimizing model-related uncertainties. In the second set, the heating sensitivity experiment (HEATING) is also forced using the climatological SST and sea ice annual cycle spanning 1979–2024. In addition, the anomalous diabatic heating is added over the ISM rainfall index region (red box in Fig. 1a, 10°N–28°N, 70°E–100°E) during boreal summer (JJA) in the

HEATING experiment. The heating rate is the observed JJA climatological average diabatic heating (Supplementary Fig. 7). We also run the HEATING experiment freely for 30 years, using the initial 5 years as spin-up. The subsequent 25 years are then averaged to form an ensemble mean, which is compared with the last 25 years ensemble mean of the CTL experiment.

Statistical information

Statistical significance testing for the Pearson correlation coefficients and linear regression between two autocorrelated time series is performed via a two-tailed Student's t-test. This research utilizes data for the climatological baseline from 1979 to 2024. We define the June–August (JJA) as boreal summer and austral winter.

Data availability

All datasets utilized in this study are freely accessible online. The ERA5 atmospheric reanalysis data can be obtained from ECMWF via https://doi.org/10.24381/cds.6860a573 and https://doi.org/10.24381/cds.f17050d7. The Hadley Centre Sea Ice and Sea Surface Temperature data set is derived at https://www.metoffice.gov.uk/hadobs/hadisst/data/download.html.

Code availability

The main codes for calculations and plotting in this study are available at: https://github.com/SongQiangH/ISM_impact_Antarctica.

Received: 25 June 2025; Accepted: 21 August 2025;
Published online: 01 September 2025

References

1. Steig, E. J. et al. Warming of the Antarctic ice-sheet surface since the 1957 International Geophysical Year. *Nature* **457**, 459–462 (2009).
2. Clem, K. R. et al. Record warming at the South Pole during the past three decades. *Nat. Clim. Chang.* **10**, 762–770 (2020).
3. Turner, J. et al. Absence of 21st century warming on Antarctic Peninsula consistent with natural variability. *Nature* **535**, 411–415 (2016).
4. Turner, J. et al. Antarctic climate change during the last 50 years. *Int. J. Climatol.* **25**, 279–294 (2005).
5. Li, X., Holland, D. M., Gerber, E. P. & Yoo, C. Impacts of the north and tropical Atlantic Ocean on the Antarctic Peninsula and sea ice. *Nature* **505**, 538–542 (2014).
6. Bromwich, D. H. et al. Central West Antarctica among the most rapidly warming regions on Earth. *Nat. Geosci.* **6**, 139–145 (2013).
7. Goosse, H., Dalaiden, Q., Feba, F., Mezzina, B. & Fogt, R. L. A drop in Antarctic sea ice extent at the end of the 1970s. *Commun. Earth Environ.* **5**, 628 (2024).
8. Holland, P. R. & Kwok, R. Wind-driven trends in Antarctic sea-ice drift. *Nat. Geosci.* **5**, 872–875 (2012).
9. Stammerjohn, S., Massom, R., Rind, D. & Martinson, D. Regions of rapid sea ice change: An inter-hemispheric seasonal comparison. *Geophys. Res. Lett.* **39**, 2012GL050874 (2012.).
10. Meehl, G. A., Chung, C. T. Y., Arblaster, J. M., Holland, M. M. & Bitz, C. M. Tropical Decadal Variability and the Rate of Arctic Sea Ice Decrease. *Geophys. Res. Lett.* **45**, 11–326 (2018).
11. Li, X. et al. Tropical teleconnection impacts on Antarctic climate changes. *Nat. Rev. Earth Environ.* **2**, 680–698 (2021).
12. Jacobs, S. S. & Comiso, J. C. Climate variability in the Amundsen and Bellingshausen Seas. *J. Clim.* **10**, 697–709 (1997).
13. Smith, R. C. & Stammerjohn, S. E. Variations of surface air temperature and sea-ice extent in the western Antarctic Peninsula region. *Ann. Glaciol.* **33**, 493–500 (2001).
14. Yuan, X. & Martinson, D. G. Antarctic sea ice extent variability and its global connectivity*. *J. Clim.* **13**, 1697–1717 (2000).
15. Jones, J. M. et al. Assessing recent trends in high-latitude Southern Hemisphere surface climate. *Nat. Clim. Change* **6**, 917–926 (2016).
16. Hobbs, W. R. et al. A review of recent changes in Southern Ocean sea ice, their drivers and forcings. *Glob. Planet. Change* **143**, 228–250 (2016).
17. Parkinson, C. L. & DiGirolamo, N. E. Sea ice extents continue to set new records: Arctic, Antarctic, and global results. *Remote Sens. Environ.* **267**, 112753 (2021).
18. Purich, A. & Doddridge, E. W. Record low Antarctic sea ice coverage indicates a new sea ice state. *Commun. Earth Environ.* **4**, 314 (2023).
19. Eayrs, C., Li, X., Raphael, M. N. & Holland, D. M. Rapid decline in Antarctic sea ice in recent years hints at future change. *Nat. Geosci.* **14**, 460–464 (2021).
20. Josey, S. A. et al. Record-low Antarctic sea ice in 2023 increased ocean heat loss and storms. *Nature* **636**, 635–639 (2024).
21. Thomas, R. et al. Accelerated Sea-Level Rise from West Antarctica. *Science* **306**, 255–258 (2004).
22. DeConto, R. M. & Pollard, D. Contribution of Antarctica to past and future sea-level rise. *Nature* **531**, 591–597 (2016).
23. Roland, T. P. et al. Sustained greening of the Antarctic Peninsula observed from satellites. *Nat. Geosci.* **17**, 1121–1126 (2024).
24. Sahade, R. et al. Climate change and glacier retreat drive shifts in an Antarctic benthic ecosystem. *Sci. Adv.* **1**, e1500050 (2015).
25. England, M. R., Polvani, L. M., Sun, L. & Deser, C. Tropical climate responses to projected Arctic and Antarctic sea-ice loss. *Nat. Geosci.* **13**, 275–281 (2020).
26. Kidston, J., Taschetto, A. S., Thompson, D. W. J. & England, M. H. The influence of Southern Hemisphere sea-ice extent on the latitude of the mid-latitude jet stream. *Geophys. Res. Lett.* **38**, 2011GL048056 (2011).
27. Haumann, F. A., Gruber, N., Münnich, M., Frenger, I. & Kern, S. Sea-ice transport driving Southern Ocean salinity and its recent trends. *Nature* **537**, 89–92 (2016).
28. Ohshima, K. I. et al. Antarctic Bottom Water production by intense sea-ice formation in the Cape Darnley polynya. *Nat. Geosci.* **6**, 235–240 (2013).
29. Lefebvre, W., Goosse, H., Timmermann, R. & Fichefet, T. Influence of the Southern Annular Mode on the sea ice–ocean system. *J. Geophys. Res.* **109**, 2004JC002403 (2004).
30. White, W. B. & Peterson, R. G. An Antarctic circumpolar wave in surface pressure, wind, temperature and sea-ice extent. *Nature* **380**, 699–702 (1996).
31. Yuan, X. & Li, C. Climate modes in southern high latitudes and their impacts on Antarctic sea ice. *J. Geophys. Res.* **113**, 2006JC004067 (2008).
32. Hobbs, W. et al. Observational evidence for a regime shift in summer Antarctic Sea Ice. *J. Clim.* **37**, 2263–2275 (2024).
33. Raphael, M. N. The influence of atmospheric zonal wave three on Antarctic sea ice variability. *J. Geophys. Res.* **112**, 2006JD007852 (2007).
34. Gloersen, P. Modulation of hemispheric sea-ice cover by ENSO events. *Nature* **373**, 503–506 (1995).
35. Welhouse, L. J., Lazzara, M. A., Keller, L. M., Tripoli, G. J. & Hitchman, M. H. Composite analysis of the effects of ENSO events on Antarctica. *J. Clim.* **29**, 1797–1808 (2016).
36. Turner, J. The El Niño–southern oscillation and Antarctica. *Int. J. Climatol.* **24**, 1–31 (2004).
37. Ding, Q., Steig, E. J., Battisti, D. S. & Küttel, M. Winter warming in West Antarctica caused by central tropical Pacific warming. *Nat. Geosci.* **4**, 398–403 (2011).
38. Clem, K. R., Renwick, J. A., McGregor, J. & Fogt, R. L. The relative influence of ENSO and SAM on Antarctic Peninsula climate. *JGR Atmos.* **121**, 9324–9341 (2016).
39. Simpkins, G. R., Peings, Y. & Magnusdottir, G. Pacific influences on tropical atlantic teleconnections to the southern hemisphere high latitudes. *J. Clim.* **29**, 6425–6444 (2016).

40. Li, X., Xie, S.-P., Gille, S. T. & Yoo, C. Atlantic-induced pan-tropical climate change over the past three decades. *Nat. Clim. Change* **6**, 275–279 (2016).
41. Li, X., Gerber, E. P., Holland, D. M. & Yoo, C. A Rossby Wave Bridge from the Tropical Atlantic to West Antarctica. *J. Clim.* **28**, 2256–2273 (2015).
42. Simpkins, G. R., McGregor, S., Taschetto, A. S., Ciasto, L. M. & England, M. H. Tropical connections to climatic change in the extratropical southern hemisphere: the role of Atlantic SST trends. *J. Clim.* **27**, 4923–4936 (2014).
43. Chen, B., Wang, C., Zhang, L. & Fan, H. Distinct impacts of the Central and Eastern Atlantic Niño on West Antarctic Sea Ice. *npj Clim. Atmos. Sci.* **8**, 142 (2025).
44. Zhang, P. & Duan, A. Connection between the Tropical Pacific and Indian Ocean and Temperature Anomaly across West Antarctic. *npj Clim. Atmos. Sci.* **6**, 49 (2023).
45. Nuncio, M. & Yuan, X. The Influence of the Indian Ocean Dipole on Antarctic Sea Ice*. *J. Clim.* **28**, 2682–2690 (2015).
46. Wang, G. et al. Compounding tropical and stratospheric forcing of the record low Antarctic sea-ice in 2016. *Nat. Commun.* **10**, 13 (2019).
47. Chen, J., Hu, X., Yang, S., Lin, S. & Li, Z. Influence of convective heating over the Maritime Continent on the West Antarctic Climate. *Geophys. Res. Lett.* **49**, e2021GL097322 (2022).
48. Holland, M. M., Landrum, L., Raphael, M. N. & Kwok, R. The regional, seasonal, and lagged influence of the Amundsen Sea Low on Antarctic Sea Ice. *Geophys. Res. Lett.* **45**, 11–227 (2018).
49. Turner, J., Phillips, T., Hosking, J. S., Marshall, G. J. & Orr, A. The Amundsen Sea low. *Int. J. Climatol.* **33**, 1818–1829 (2013).
50. Raphael, M. N. et al. The Amundsen sea low: variability, change, and impact on Antarctic Climate. *Bull. Am. Meteorol. Soc.* **97**, 111–121 (2016).
51. Dou, J. & Zhang, R. Impact of sea surface temperature in the extratropical Southern Indian Ocean on Antarctic Sea Ice in Austral Spring. *J. Clim.* **36**, 8259–8275 (2023).
52. Xiao, C., Duan, A., Yao, Y., Tang, Y. & Wang, Q. Role of the subtropical southern Indian Ocean in the interannual variability of Antarctic summer sea ice. *Atmos. Res.* **311**, 107723 (2024).
53. Liu, Y. et al. Decadal oscillation provides skillful multiyear predictions of Antarctic sea ice. *Nat. Commun.* **14**, 8286 (2023).
54. Li, X., Holland, D. M., Gerber, E. P. & Yoo, C. Rossby Waves Mediate Impacts of Tropical Oceans on West Antarctic Atmospheric Circulation in Austral Winter. *J. Clim.* **28**, 8151–8164 (2015).
55. Purich, A., Cai, W., England, M. H. & Cowan, T. Evidence for link between modelled trends in Antarctic sea ice and underestimated westerly wind changes. *Nat. Commun.* **7**, 10409 (2016).
56. Meehl, G. A., Arblaster, J. M., Bitz, C. M., Chung, C. T. Y. & Teng, H. Antarctic sea-ice expansion between 2000 and 2014 driven by tropical Pacific decadal climate variability. *Nat. Geosci.* **9**, 590–595 (2016).
57. Man, K. et al. Century-long West Antarctic snow accumulation changes induced by tropical teleconnections. *Sci. Adv* **11**, eadr2821 (2025).
58. Wille, J. D. et al. Atmospheric rivers in Antarctica. *Nat. Rev. Earth Environ.* **6**, 178–192 (2025).
59. Clem, K. R., Bozkurt, D., Kennett, D., King, J. C. & Turner, J. Central tropical Pacific convection drives extreme high temperatures and surface melt on the Larsen C Ice Shelf, Antarctic Peninsula. *Nat. Commun.* **13**, 3906 (2022).
60. Baiman, R. et al. Synoptic and planetary-scale dynamics modulate Antarctic atmospheric river precipitation intensity. *Commun. Earth Environ.* **5**, 127 (2024).
61. Shields, C. A., Wille, J. D., Marquardt Collow, A. B., Maclennan, M. & Gorodetskaya, I. V. Evaluating uncertainty and modes of variability for Antarctic Atmospheric Rivers. *Geophys. Res. Lett* **49**, e2022GL099577 (2022).
62. Gadgil, S. The indian monsoon and its variability. *Annu. Rev. Earth Planet. Sci.* **31**, 429–467 (2003).
63. Chatterjee, S., Ravichandran, M., Murukesh, N., Raj, R. P. & Johannessen, O. M. A possible relation between Arctic sea ice and late season Indian Summer Monsoon Rainfall extremes. *npj Clim. Atmos. Sci.* **4**, 36 (2021).
64. Prabhu, A., Mandke, S. K., Kripalani, R. H. & Pandithurai, G. Association between Antarctic Sea ice, Pacific SST and the Indian summer monsoon: an observational study. *Polar Sci.* **30**, 100746 (2021).
65. Chandra, V., Sandeep, S., Suhas, E. & Subramanian, A. C. Weakening of indian summer monsoon synoptic activity in response to polar sea ice melt induced by albedo reduction in a climate model. *Earth Space Sci.* **9**, e2021EA002185 (2022).
66. Chandra, V. & Sandeep, S. Relative roles of the Arctic and Antarctic sea ice melt on Indian summer monsoon. *Clim. Dyn.* **62**, 5373–5387 (2024).
67. Zhu, J. & Wu, Z. Indian summer monsoon's role in shaping variability in Arctic sea ice. *npj Clim. Atmos. Sci.* **7**, 1–15 (2024).
68. Grunseich, G. & Wang, B. Arctic Sea ice patterns driven by the Asian summer monsoon. *J. Clim.* **29**, 9097–9112 (2016).
69. Lin, H. Global extratropical response to diabatic heating variability of the Asian summer monsoon. *J. Atmos. Sci.* **66**, 2697–2713 (2009).
70. Rodwell, M. J. & Hoskins, B. J. Monsoons and the dynamics of deserts. *Q. J. R. Met. Soc.* **122**, 1385–1404 (1996).
71. Ding, Q. & Wang, B. Circumglobal teleconnection in the Northern Hemisphere summer. *J. Clim.* **18**, 3483–3505 (2005).
72. Tang, S. et al. Linkages of unprecedented 2022 Yangtze River Valley heatwaves to Pakistan flood and triple-dip La Niña. *npj Clim. Atmos. Sci.* **6**, 44 (2023).
73. Fu, Z.-H., Zhou, W., Xie, S.-P., Zhang, R. & Wang, X. Dynamic pathway linking Pakistan flooding to East Asian heatwaves. *Sci. Adv.* **10**, eadk9250 (2024).
74. Song, Q., Wang, C., Yao, Y. & Fan, H. Unraveling the Indian monsoon's role in fueling the unprecedented 2022 Marine Heatwave in the Western North Pacific. *npj Clim. Atmos. Sci.* **7**, 90 (2024).
75. Stokes, C. R. et al. Response of the East Antarctic Ice Sheet to past and future climate change. *Nature* **608**, 275–286 (2022).
76. Gadgil, S., Vinayachandran, P. N., Francis, P. A. & Gadgil, S. Extremes of the Indian summer monsoon rainfall, ENSO and equatorial Indian Ocean oscillation. *Geophys. Res. Lett.* **31**, L12213 (2004).
77. Ashok, K. & Tejavath, C. T. The Indian summer monsoon rainfall and ENSO. *MAUSAM* **70**, 443–452 (2021).
78. Frederiksen, J. S. & Bell, R. C. Teleconnection patterns and the roles of baroclinic, barotropic and topographic instability. *J. Atmos. Sci.* **44**, 2200–2218 (1987).
79. Horel, J. D. & Wallace, J. M. Planetary-scale atmospheric phenomena associated with the southern oscillation. *Mon. Wea. Rev.* **109**, 813–829 (1981).
80. Simmons, A. J., Wallace, J. M. & Branstator, G. W. Barotropic wave propagation and instability, and atmospheric teleconnection patterns. *J. Atmos. Sci.* **40**, 1363–1392 (1983).
81. Sardeshmukh, P. D. & Hoskins, B. J. The generation of global rotational flow by steady idealized tropical divergence. *J. Atmos. Sci.* **45**, 1228–1251 (1988).
82. Atiqah Azhar, S. S., Chenoli, S. N., Samah, A. A. & Kim, S.-J. The linkages between Antarctic sea ice extent and Indian summer monsoon rainfall. *Polar Sci.* **25**, 100537 (2020).
83. Azhar, S. S. A., Chenoli, S. N., Samah, A. A., Kim, S.-J. & Murukesh, N. The mechanism linking the variability of the Antarctic sea ice extent in the Indian Ocean sector to Indian summer monsoon rainfall. *Clim. Dyn.* **60**, 2665–2685 (2023).
84. Turner, A. G. & Annamalai, H. Climate change and the South Asian summer monsoon. *Nat. Clim. Change* **2**, 587–595 (2012).

85. Sharmila, S., Joseph, S., Sahai, A. K., Abhilash, S. & Chattopadhyay, R. Future projection of Indian summer monsoon variability under climate change scenario: an assessment from CMIP5 climate models. *Glob. Planet. Change* **124**, 62–78 (2015).
86. Maharana, P., Dimri, A. P. & Choudhary, A. Future changes in Indian summer monsoon characteristics under 1.5 and 2 °C specific warming levels. *Clim. Dyn.* **54**, 507–523 (2020).
87. Stocker, T. *Climate Change 2013: The Physical Science Basis: Working Group I Contribution to the Fifth Assessment Report of the Intergovernmental Panel on Climate Change*. (Cambridge university press, 2014).
88. Hersbach, H. et al. The ERA5 global reanalysis. *Quart. J. R. Meteor. Soc.* **146**, 1999–2049 (2020).
89. Rayner, N. A. et al. Global analyses of sea surface temperature, sea ice, and night marine air temperature since the late nineteenth century. *J. Geophys. Res.* **108**, 2002JD002670 (2003).
90. Takaya, K. & Nakamura, H. A formulation of a phase-independent wave-activity flux for stationary and migratory quasigeostrophic eddies on a zonally varying basic flow. *J. Atmos. Sci.* **58**, 608–627 (2001).
91. Yanai, M., Esbensen, S. & Chu, J.-H. Determination of bulk properties of tropical cloud clusters from large-scale heat and moisture budgets. *J. Atmos. Sci.* **30**, 611–627 (1973).
92. Yanai, M., Li, C. & Song, Z. Seasonal heating of the Tibetan Plateau and its effects on the evolution of the Asian summer monsoon. *J. Meteorol. Soc. Jpn. Ser. II* **70**, 319–351 (1992).
93. Neale, R. B. et al. Description of the NCAR Community Atmosphere Model (CAM 5.0). *NCAR Tech. Note NCAR/TN-486+STR* **1**, 1–12 (2010).
94. Li, X., Zheng, J., Wang, C., Lin, X. & Yao, Z. Unraveling the roles of jet streams on the unprecedented hot July in Western Europe in 2022. *npj Clim. Atmos. Sci* **7**, 323 (2024).

Acknowledgements

This study was funded by the National Natural Science Foundation of China (W2441014, 42192560, and 42106202) and the development fund of the South China Sea Institute of Oceanology, Chinese Academy of Sciences (SCSIO202208). Numerical simulations were conducted with support from the High Performance Computing Division at the South China Sea Institute of Oceanology. We are grateful for the valuable suggestions provided by Dr. Yulong Yao and Ms. Wenjie Yi from South China Sea Institute of Oceanology. We also thank Dr. Zilu Meng from University of Washington for developing the python package "Sacpy", which facilitated our research. We sincerely thank the two anonymous reviewers for their valuable comments and suggestions on our research.

Author contributions

Q.S. and C.W. proposed and conceived the study. C.W. and L.Z. contributed to the research design, offered feedback, and assisted in revising the manuscript. Q.S. and H.F. performed the numerical simulations. All authors (Q.S., C.W., L.Z., and H.F.) read and approved the final manuscript.

Competing interests

The authors declare no competing interests.

Additional information

Supplementary information The online version contains supplementary material available at https://doi.org/10.1038/s41612-025-01213-7.

Correspondence and requests for materials should be addressed to Chunzai Wang.

Reprints and permissions information is available at http://www.nature.com/reprints

Publisher's note Springer Nature remains neutral with regard to jurisdictional claims in published maps and institutional affiliations.

Open Access This article is licensed under a Creative Commons Attribution 4.0 International License, which permits use, sharing, adaptation, distribution and reproduction in any medium or format, as long as you give appropriate credit to the original author(s) and the source, provide a link to the Creative Commons licence, and indicate if changes were made. The images or other third party material in this article are included in the article's Creative Commons licence, unless indicated otherwise in a credit line to the material. If material is not included in the article's Creative Commons licence and your intended use is not permitted by statutory regulation or exceeds the permitted use, you will need to obtain permission directly from the copyright holder. To view a copy of this licence, visit http://creativecommons.org/licenses/by/4.0/.

© The Author(s) 2025